IEICE TRANS. FUNDAMENTALS, VOL.E87–A, NO.3 MARCH 2004

PAPER Special Section on Applications and Implementations of Digital Signal Processing

A Fingerprint Matching Algorithm Using Phase-Only Correlation

Koichi ITO[†a)], ***Student Member***, **Hiroshi NAKAJIMA**[††], ***Nonmember***, **Koji KOBAYASHI**[††], **Takafumi AOKI**[†], ***Members***, ***and*** **Tatsuo HIGUCHI**[†††], ***Fellow***

SUMMARY This paper presents an algorithm for fingerprint matching using the Phase-Only Correlation (POC) function. One of the most difficult problems in human identification by fingerprints has been that the matching performance is significantly influenced by fingertip surface condition, which may vary depending on environmental or personal causes. This paper proposes a new fingerprint matching algorithm using phase spectra of fingerprint images. The proposed algorithm is highly robust against fingerprint image degradation due to inadequate fingertip conditions. A set of experiments is carried out using fingerprint images captured by a pressure sensitive fingerprint sensor. The proposed algorithm exhibits efficient identification performance even for difficult fingerprint images that could not be identified by the conventional matching algorithms.

key words: *phase-only correlation, phase-only matched filtering, phase correlation, biometrics, fingerprint verification, fingerprint identification*

1. Introduction

Human body has a complicated three-dimensional structure, whose condition varies considerably according to environmental or internal conditions. The goal of image-based biometrics is, regardless of which biometric trait is used, to identify a person as precise as possible without being affected by image variations per each trial. Compared with industrial image recognition, biometrics applications require much more robust image preprocessing as well as more precise image recognition.

A fingerprint is a representation of the epidermis of a finger being composed of a set of ridges and furrows. The uniqueness of a fingerprint can be determined by the pattern of ridges and furrows as well as the minutiae points (i.e., ridge ending and ridge bifurcation). Among all the biometric techniques, fingerprint-based identification [1] is the most popular method, which has been successfully used in many applications. Typical fingerprint identification methods employ feature-based image matching, where ridge lines in the original fingerprint image are thinned by image preprocessing, minutiae points in the ridge lines are identified, and line orientation or the number of lines between every pair of minutiae points is calculated [1]–[3]. These features are used for identifying a valid fingerprint image. The feature-based matching provides an effective way of identification for majority of people. However, it has been known that there are a number of people whose fingerprints could not be identified by the feature-based methods due to special skin conditions, where feature points are hard to be extracted by image processing. The ratio of people who have such difficult fingerprints varies depending on race, sex, age, job groupings, etc., but it is said that one to five percentage of total population may fall into this category.

Addressing this problem, this paper proposes an efficient fingerprint matching algorithm using a Phase-Only Correlation (POC) function (or simply a "phase-correlation function") [4]–[6]. The POC technique has been successfully applied to high-accuracy image registration tasks for computer vision applications [7]–[9], where estimation of sub-pixel image translation is a major concern. In this paper, we demonstrate that the POC technique is also effective for fingerprint matching (see [5] for earlier discussions of this approach).

This paper is organized as follows: Sect. 2 gives the definition of the POC function and its basic properties. Section 3 defines a *band-limited POC* function for fingerprint matching. Section 4 describes a fingerprint matching algorithm using the band-limited POC function. Section 5 presents a set of experiments for evaluating matching performance of the proposed algorithm and compares it with that of the conventional matching algorithm. In Sect. 5, we end with some conclusions.

2. Phase-Only Correlation (POC)

This section shows the definition of a Phase-Only Correlation (POC) function.

Consider two $N_1 \times N_2$ images, $f(n_1, n_2)$ and $g(n_1, n_2)$, where we assume that the index ranges are $n_1 = -M_1 \cdots M_1$ ($M_1 > 0$) and $n_2 = -M_2 \cdots M_2$ ($M_2 > 0$) for mathematical simplicity, and hence $N_1 = 2M_1 + 1$ and $N_2 = 2M_2 + 1$. Let $F(k_1, k_2)$ and $G(k_1, k_2)$ denote the 2D Discrete Fourier Transforms (2D DFTs) of the two images. $F(k_1, k_2)$ and $G(k_1, k_2)$ are given by

$$\begin{aligned} F(k_1, k_2) &= \sum_{n_1, n_2} f(n_1, n_2) W_{N_1}^{k_1 n_1} W_{N_2}^{k_2 n_2} \\ &= A_F(k_1, k_2) e^{j\theta_F(k_1, k_2)}, \end{aligned} \tag{1}$$

Manuscript received July 3, 2003.
Manuscript revised October 6, 2003.
Final manuscript received November 25, 2003.

[†]The authors are with the Department of Computer and Mathematical Sciences, Graduate School of Information Sciences, Tohoku University, Sendai-shi, 980-8579 Japan.
[††]The authors are with Yamatake Corporation, Isehara-shi, 259-1195 Japan.
[†††]The author is with the Department of Electronics, Tohoku Institute of Technology, Sendai-shi, 982-8577 Japan.
a) E-mail: ito@aoki.ecei.tohoku.ac.jp

$$G(k_1, k_2) = \sum_{n_1,n_2} g(n_1, n_2) W_{N_1}^{k_1 n_1} W_{N_2}^{k_2 n_2} = A_G(k_1, k_2) e^{j\theta_G(k_1,k_2)}, \quad (2)$$

where $k_1 = -M_1 \cdots M_1$, $k_2 = -M_2 \cdots M_2$, $W_{N_1} = e^{-j\frac{2\pi}{N_1}}$, $W_{N_2} = e^{-j\frac{2\pi}{N_2}}$, and the operator $\sum_{n_1,n_2}$ denotes $\sum_{n_1=-M_1}^{M_1} \sum_{n_2=-M_2}^{M_2}$. $A_F(k_1, k_2)$ and $A_G(k_1, k_2)$ are amplitude components, and $e^{j\theta_F(k_1,k_2)}$ and $e^{j\theta_G(k_1,k_2)}$ are phase components. The cross spectrum $R_{FG}(k_1, k_2)$ between $F(k_1, k_2)$ and $G(k_1, k_2)$ is given by

$$R_{FG}(k_1, k_2) = F(k_1, k_2)\overline{G(k_1, k_2)} = A_F(k_1, k_2) A_G(k_1, k_2) e^{j\theta(k_1,k_2)}, \quad (3)$$

where $\overline{G(k_1, k_2)}$ denotes the complex conjugate of $G(k_1, k_2)$ and $\theta(k_1, k_2)$ denotes the phase difference $\theta_F(k_1, k_2) - \theta_G(k_1, k_2)$. The ordinary correlation function $r_{fg}(n_1, n_2)$ is the 2D Inverse Discrete Fourier Transform (2D IDFT) of $R_{FG}(k_1, k_2)$ and is given by

$$r_{fg}(n_1, n_2) = \frac{1}{N_1 N_2} \sum_{k_1,k_2} R_{FG}(n_1, n_2) W_{N_1}^{-k_1 n_1} W_{N_2}^{-k_2 n_2}, \quad (4)$$

where $\sum_{k_1 k_2}$ denotes $\sum_{k_1=-M_1}^{M_1} \sum_{k_2=-M_2}^{M_2}$.

On the other hand, the cross-phase spectrum (or normalized cross spectrum) $\hat{R}_{FG}(k_1, k_2)$ is defined as

$$\hat{R}_{FG}(k_1, k_2) = \frac{F(k_1, k_2)\overline{G(k_1, k_2)}}{|F(k_1, k_2)\overline{G(k_1, k_2)}|} = e^{j\theta(k_1,k_2)}. \quad (5)$$

The POC function $\hat{r}_{fg}(n_1, n_2)$ is 2D IDFT of $\hat{R}_{FG}(k_1, k_2)$ and is given by

$$\hat{r}_{fg}(n_1, n_2) = \frac{1}{N_1 N_2} \sum_{k_1,k_2} \hat{R}_{FG}(k_1, k_2) W_{N_1}^{-k_1 n_1} W_{N_2}^{-k_2 n_2}. \quad (6)$$

When $f(n_1, n_2)$ and $g(n_1, n_2)$ are the same image, i.e., $f(n_1, n_2) = g(n_1, n_2)$, the POC function will be given by

$$\hat{r}_{ff}(n_1, n_2) = \frac{1}{N_1 N_2} \sum_{k_1,k_2} W_{N_1}^{-k_1 n_1} W_{N_2}^{-k_2 n_2} = \delta(n_1, n_2) = \begin{cases} 1 & \text{if } n_1 = n_2 = 0 \\ 0 & \text{otherwise.} \end{cases} \quad (7)$$

The above equation implies that the POC function between two identical images is the Kronecker's delta function $\delta(n_1, n_2)$.

The most remarkable property of POC compared to the ordinary correlation is its accuracy in image matching. Figure 1 shows an example of image matching using the POC function. When two images are similar, their POC function $\hat{r}(n_1, n_2)$ gives a distinct sharp peak. When two images are not similar, the peak drops significantly. Thus, the POC function exhibits much higher discrimination capability than the ordinary correlation function. The height of the peak can be used as a good similarity measure for image matching.

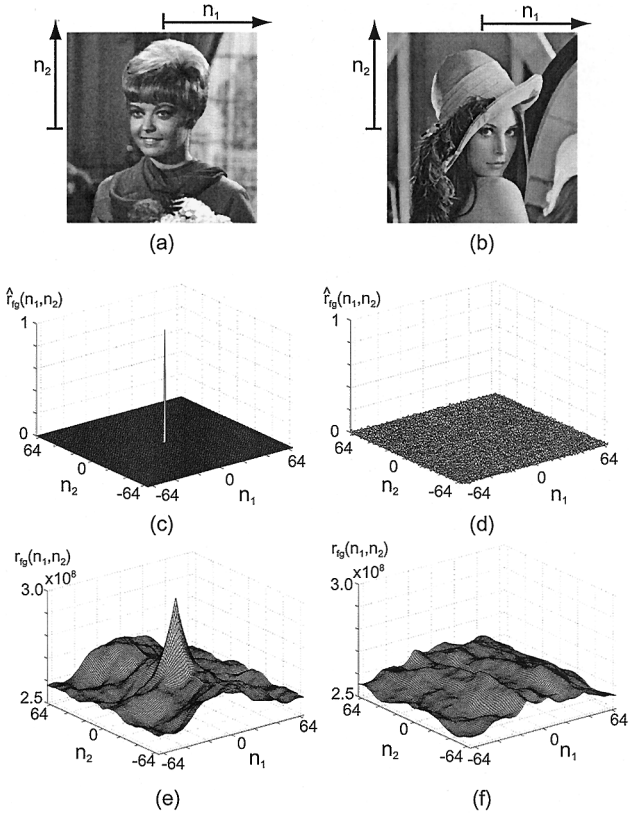

Fig. 1 Examples of the POC function $\hat{r}_{fg}(n_1, n_2)$ and the ordinary correlation function $r_{fg}(n_1, n_2)$: (a) image $f(n_1, n_2)$, (b) image $g(n_1, n_2)$, (c) POC function between the two identical images (the image $f(n_1, n_2)$), (d) POC function between $f(n_1, n_2)$ and $g(n_1, n_2)$, (e) ordinary correlation function between the two identical images (the image $f(n_1, n_2)$), and (f) ordinary correlation function between $f(n_1, n_2)$ and $g(n_1, n_2)$.

Other important properties of the POC function used for fingerprint matching is that it is not influenced by image shift and brightness change, and it is highly robust against noise.

(i) Property of shift invariance

Let $g_1(n_1, n_2)$ be the displaced version of the original image $g(n_1, n_2)$. Then, $g_1(n_1, n_2)$ is given by

$$g_1(n_1, n_2) = g(n_1 + \tau_1, n_2 + \tau_2), \quad (8)$$

where (τ_1, τ_2) are the displacements. The POC function $\hat{r}_{fg_1}(n_1, n_2)$ between $f(n_1, n_2)$ and $g_1(n_1, n_2)$ will be given by

$$\hat{r}_{fg_1}(n_1, n_2) = \frac{1}{N_1 N_2} \sum_{k_1,k_2} e^{j\{\theta(k_1,k_2) - \frac{2\pi\tau_1 n_1}{N_1} - \frac{2\pi\tau_2 n_2}{N_2}\}} \times W_{N_1}^{-k_1 n_1} W_{n_2}^{-k_2 n_2} \cong \hat{r}_{fg}(n_1 + \tau_1, n_2 + \tau_2). \quad (9)$$

The above equation shows that the correlation peak is shifted by (τ_1, τ_2) and the value of the peak is invariant with respect to the positional image translation. We can estimate

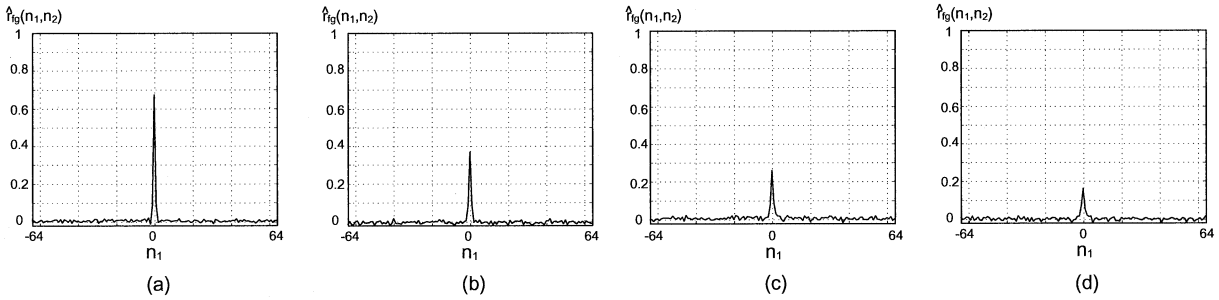

Fig. 2 POC function (showing the cross section of $n_2 = 0$) for (a) $S/N = 20$ dB, (b) $S/N = 10$ dB, (c) $S/N = 5$ dB and (d) $S/N = 0$ dB.

the image shift (τ_1, τ_2) by detecting the location of the correlation peak.

(ii) Property of brightness invariance

Suppose that $g_2(n_1, n_2)$ is the brightness-scaled image of $g(n_1, n_2)$, and is given by

$$g_2(n_1, n_2) = \alpha g(n_1, n_2), \tag{10}$$

where $\alpha > 0$. The 2D DFT $G_2(n_1, n_2)$ of $g_2(n_1, n_2)$ is given by

$$\begin{aligned} G_2(k_1, k_2) &= \sum_{n_1, n_2} \alpha g(n_1, n_2) W_{N_1}^{k_1 n_1} W_{N_2}^{k_2 n_2} \\ &= \alpha A_G(k_1, k_2) e^{j\theta_G(k_1, k_2)}. \end{aligned} \tag{11}$$

The POC function $\hat{r}_{fg_2}(n_1, n_2)$ between $f(n_1, n_2)$ and $g_2(n_1, n_2)$ is calculated as

$$\begin{aligned} \hat{r}_{fg_2}(n_1, n_2) &= \frac{1}{N_1 N_2} \sum_{k_1, k_2} \hat{R}_{FG}(k_1, k_2) W_{N_1}^{-k_1 n_1} W_{N_2}^{-k_2 n_2} \\ &= \hat{r}_{fg}(n_1, n_2). \end{aligned} \tag{12}$$

The above equation implies that the POC function is not influenced by brightness change.

(iii) Property of noise immunity

Figure 2 shows an example of the noise immunity of POC, where the POC function is calculated between the original image (a) in Fig. 1 and the same image with additive white noise of various energy. When two input images are totally same, the POC function becomes the delta function $\delta(n_1, n_2)$ having the peak value 1. When one input image contains random additive noise, the correlation peak decreases without changing its shape as noise energy increases. From this result, we can see that POC has high immunity against additive noise.

3. Band-Limited POC Function and Similarity Evaluation for Fingerprint Matching

In this section, we modify the definition of POC function to have a band-limited POC function dedicated to fingerprint matching tasks.

Our initial experimental observation shows that the POC-based image matching is quite effective for fingerprint verification [5]. The height of the correlation peak gives a good similarity measure in fingerprint matching. However, we also found that the 2D DFT of a fingerprint image sometimes includes meaningless phase components in high frequency domain, since a significant information of a fingerprint image is concentrated in an elliptic frequency band of its ridge lines. Figure 3 shows the fingerprint image and the corresponding amplitude spectrum of its 2D DFT. A typical fingerprint image has an elliptic spectral distribution in frequency domain. The frequency components that are higher than this dominant frequency components have very low power, and hence their phase components are not reliable. The cross-spectrum $\hat{R}_{FG}(k_1, k_2)$ (Eq. (5)) implies that the calculation of POC emphasizes the high frequency components, which may have less reliability (with low S/N). We observe that this reduces the height of the correlation peak significantly even if the given two fingerprint images are captured from a common fingertip.

The basic idea to improve the matching performance is to eliminate meaningless high frequency components in the calculation of cross-phase spectrum $\hat{R}_{FG}(k_1, k_2)$ depending on the frequency spectrum of the given fingerprint image. Assume that the ranges of the inherent frequency band are given by $k_1 = -K_1 \cdots K_1$ and $k_2 = -K_2 \cdots K_2$, where $0 \leqq K_1 \leqq M_1$ and $0 \leqq K_2 \leqq M_2$ as shown in Fig. 3(b). (The parameters K_1 and K_2 may be automatically detected by image processing.) Thus, the effective size of frequency spectrum is given by $L_1 = 2K_1 + 1$ and $L_2 = 2K_2 + 1$. Instead of the original POC, we use the band-limited POC function defined as

$$\begin{aligned} \hat{r}_{fg}^{K_1 K_2}(n_1, n_2) &= \frac{1}{L_1 L_2} \sum_{k_1=-K_1}^{K_1} \sum_{k_2=-K_2}^{K_2} \hat{R}_{FG}(k_1, k_2) \\ &\quad \times W_{L_1}^{-k_1 n_1} W_{L_2}^{-k_2 n_2}, \end{aligned} \tag{13}$$

where $n_1 = -K_1 \cdots K_1$ and $n_2 = -K_2 \cdots K_2$. Note that the maximum value of the correlation peak of the band-limited POC function is always normalized to 1 and is not depending on the frequency band size L_1 and L_2. The shape of the band-limited POC function for the two identical images is always the Kronecker's delta function $\delta(n_1, n_2)$. Also, note that the original POC function can be represented as $\hat{r}_{fg}(n_1, n_2) = \hat{r}_{fg}^{M_1 M_2}(n_1, n_2)$.

Another approach to define a frequency selective POC function is to apply an adequate low-pass filter to cross-

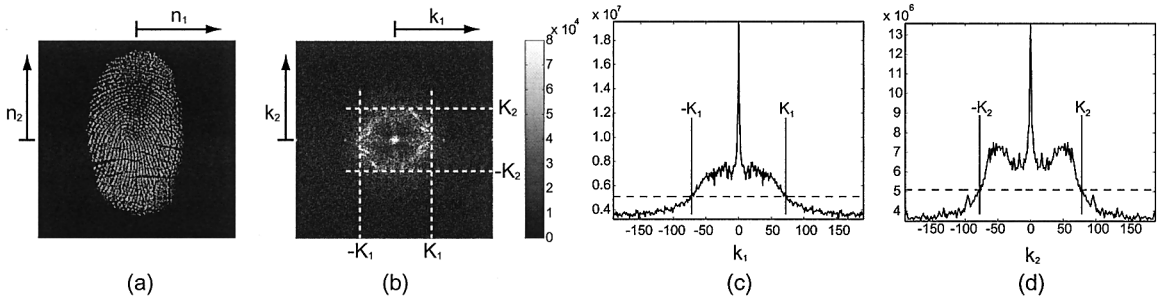

Fig. 3 Fingerprint image in space domain (a) and in frequency domain (b) (amplitude spectrum). (c) and (d) are k_2-axis and k_1-axis projection of the amplitude spectrum. The dashed lines denote the mean value for each projection.

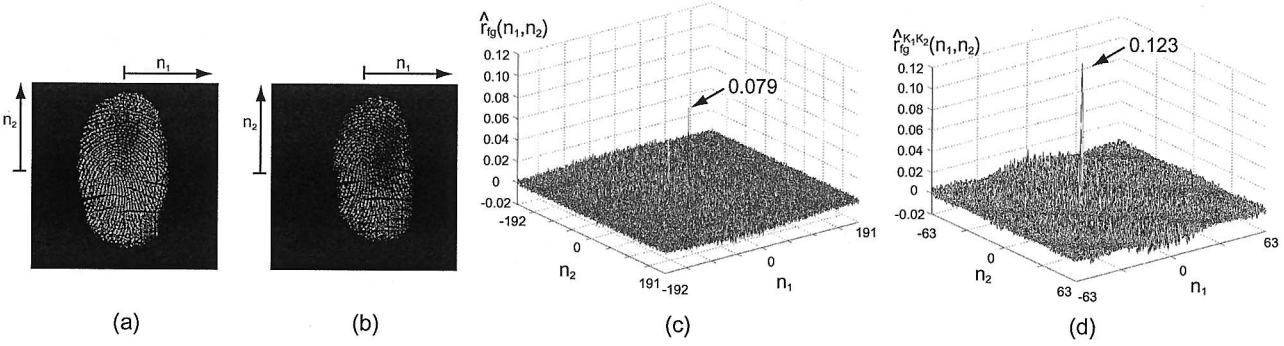

Fig. 4 Example of genuine matching using the original POC function and the band-limited POC function: (a) registered fingerprint image $f(n_1, n_2)$, (b) input fingerprint image $g(n_1, n_2)$ captured from the same fingertip, (c) original POC function $\hat{r}_{fg}(n_1, n_2)$ and (d) band-limited POC function $\hat{r}_{fg}^{K_1 K_2}(n_1, n_2)$ where $K_1 = 63$ and $K_2 = 63$.

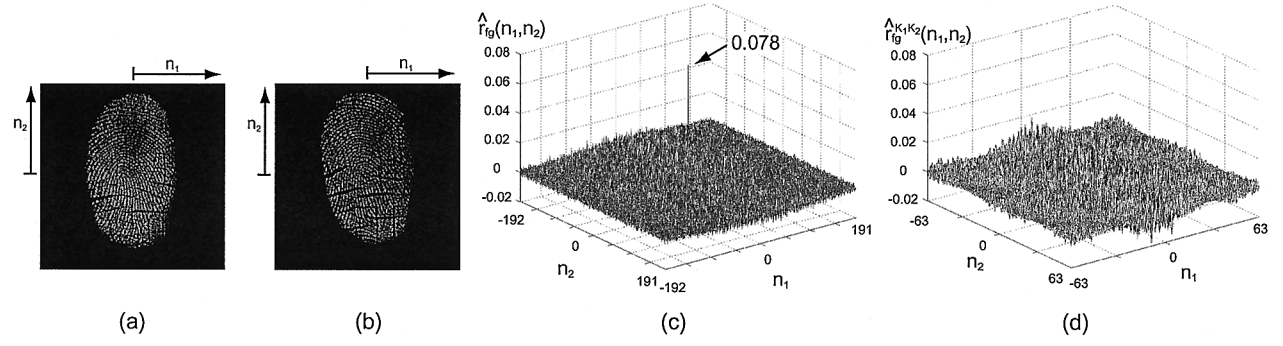

Fig. 5 Example of impostor matching using the original POC function and the band-limited POC function: (a) registered fingerprint image $f(n_1, n_2)$, (b) input fingerprint image $g(n_1, n_2)$ captured from the different fingertip, (c) original POC function $\hat{r}_{fg}(n_1, n_2)$ and (d) band-limited POC function $\hat{r}_{fg}^{K_1 K_2}(n_1, n_2)$ where $K_1 = 63$ and $K_2 = 63$.

phase spectrum $\hat{R}_{FG}(k_1, k_2)$. In this approach, however, the shape and height of the correlation peak varies depending on the type of low-pass filters [8]. Also, the evaluation of image similarity requires fitting a model peak function to the correlation data array. The band-limited POC function does not require such a complicated computation for evaluating the similarity between images.

Figures 4 and 5 show examples of genuine matching and impostor matching using the original POC function $\hat{r}_{fg}$ and the band-limited POC function $\hat{r}_{fg}^{K_1 K_2}$. In the case of genuine matching, the band-limited POC function provides the higher correlation peak than that of the original POC function. In the case of impostor matching, the band-limited POC function gives no distinct correlation peak, while the original POC function gives a peak that may cause a matching error. Thus, the band-limited POC function exhibits much higher discrimination capability than the original POC function.

A natural question is how to determine the upper limits K_1 and K_2 of the effective frequency components in a given fingerprint image. In this paper, we automatically determine K_1 and K_2 depending on the input image as follows: (i) compute the amplitude spectrum of a fingerprint image by 2D DFT (Fig. 3(b)), (ii) compute k_2-axis projection $p_{k_2}(k_1)$ and k_1-axis projection $p_{k_1}(k_2)$ of the amplitude spectrum (Figs. 3(c) and (d)), (iii) compute the mean values $\mu_{p_{k_2}}$ and $\mu_{p_{k_1}}$ for the two projections $p_{k_2}(k_1)$ and $p_{k_1}(k_2)$, respectively, and (iv) define the parameters K_1 and K_2 as

$$K_1 = \max(\{k_1 | p_{k_2}(k_1) \geqq \mu_{p_{k_2}}, 0 \leqq k_1 \leqq M_1\}), \quad (14)$$

$$K_2 = \max(\{k_2 | p_{k_1}(k_2) \geqq \mu_{p_{k_1}}, 0 \leqq k_2 \leqq M_2\}). \quad (15)$$

Note that the amplitude spectrum is even symmetric for every axis.

In many cases, however, the band-limited POC function has multiple peaks, which is caused by elastic fingerprint deformation. The fingerprint image can expand or contract when a fingertip contacts with the sensor surface. Each portion of the fingerprint image will be shifted independently, which means several sub-domains in the image are moving individually. In this case, the POC function produces several peaks corresponding to the multiple translated sub-domains. The height of every correlation peak reflects the matched area of each sub-domain. Hence, we decide to employ the sum of these peaks as an evaluation criterion in order to make the proposed matching algorithm robust against elastic deformation. In our algorithm, we employ the sum of the highest P peaks of the band-limited POC function $\hat{r}_{fg}^{K_1K_2}(n_1, n_2)$ as a matching score, which is denoted by $S_P^{K_1K_2}[f, g]$.

4. Fingerprint Matching Algorithm Using the Band-Limited POC Function

In this section, we propose the fingerprint matching algorithm using the band-limited POC function. A fingerprint matching algorithm compares the registered fingerprint and the input fingerprint, and returns either a degree of similarity or a binary decision. Matching fingerprint images is an extremely difficult problem, mainly due to the large variability in different impressions of the same finger, e.g., (i) displacement, (ii) rotation, (iii) deformation, (iv) skin condition and (v) noise. The POC-based approach is particularly robust against the above items (i), (iv) and (v). On the other hand, the image rotation (ii) must be normalized by preprocessing. We can address the fingerprint deformation (iii) due to skin plasticity by introducing multiple-peak evaluation of matching score i.e., $S_P^{K_1K_2}[f, g]$.

Figure 6 shows the fingerprint matching algorithm using the POC function. The proposed algorithm first normalizes the input image and compares it with the registered image, where the total process consists of the four steps: (i) rotation alignment, (ii) displacement alignment, (iii) common region extraction and (iv) fingerprint matching. Figure 7 illustrates the example of fingerprint matching using the proposed algorithm.

procedure *Fingerprint Matching Using POC Function*

Input:
$f(n_1, n_2)$: the registered fingerprint image,
$g(n_1, n_2)$: the fingerprint image to be verified;
Output:
matching score between $f(n_1, n_2)$ and $g(n_1, n_2)$;

1. **begin**
2. store in advance a set of rotated images $f_\theta(n_1, n_2)$ of $f(n_1, n_2)$ over the angular range $-\theta_{max} \leqq \theta \leqq \theta_{max}$ with an angle spacing 1°;
3. calculate the POC function $\hat{r}_{f_\theta g}^{M_1M_2}(n_1, n_2)$ between $f_\theta(n_1, n_2)$ and $g(n_1, n_2)$;
4. calculate $\Theta = \arg\max_\theta\{S_1^{M_1M_2}[f_\theta, g]\}$ to select the rotation-normalized image $f_\Theta(n_1, n_2)$;
5. estimate image displacements (τ_1, τ_2) between $f_\Theta(n_1, n_2)$ and $g(n_1, n_2)$ from the peak location of $\hat{r}_{f_\Theta g}^{M_1M_2}(n_1, n_2)$;
6. extend the size of $f_\Theta(n_1, n_2)$ and $g(n_1, n_2)$ by τ_1 and τ_2 pixels for n_1 and n_2 directions to obtain $f'(n_1, n_2)$ and $g'(n_1, n_2)$;
7. extract the effective fingerprint regions $f''(n_1, n_2)$ and $g''(n_1, n_2)$ from $f'(n_1, n_2)$ and $g'(n_1, n_2)$;
8. detect the inherent frequency band (K_1, K_2) from the 2D DFT of $f''(n_1, n_2)$;
9. calculate the band-limited POC function $\hat{r}_{f''g''}^{K_1K_2}(n_1, n_2)$;
10. compute the matching score $S_P^{K_1K_2}[f'', g'']$
11. **end**.

Fig. 6 Fingerprint matching algorithm using the POC function.

(i) Rotation alignment (lines 2–4)

The POC function is sensitive to the image rotation, and hence we need to normalize the rotation angle between the registered fingerprint $f(n_1, n_2)$ and the input fingerprint $g(n_1, n_2)$ in order to perform the high-accuracy fingerprint matching. Our experimental observation shows that rotation alignment of less than $\pm 1°$ must be performed for high-accuracy fingerprint matching using the POC function. The proposed algorithm employs a straightforward approach for rotation estimation. We first generate a set rotated images $f_\theta(n_1, n_2)$ of the registered fingerprint $f(n_1, n_2)$ over the angular range $-\theta_{max} \leqq \theta \leqq \theta_{max}$ with an angle spacing 1°, where bi-cubic interpolation is employed for image rotation. We use $\theta_{max} = 20°$ in our experiment. The rotation angle Θ of the input image is determined by evaluating the similarity between the registered image $f_\theta(n_1, n_2)$ $(-\theta_{max} \leqq \theta \leqq \theta_{max})$ and the input image $g(n_1, n_2)$ using POC function. In our experiments, we use the following formula:

$$\Theta = \arg\max_\theta\{S_1^{M_1M_2}[f_\theta, g]\}. \quad (16)$$

In practical situation, we store in advance a set of rotated versions of the registered image into a memory in order to reduce the processing time. We calculate the POC function $\hat{r}_{f_\theta g}^{M_1M_2}(n_1, n_2)$ between the rotated image $f_\theta(n_1, n_2)$ and the input $g(n_1, n_2)$, and find the highest correlation peak. The rotated image $f_\Theta(n_1, n_2)$ that gives the highest correlation peak is selected as the rotation-normalized image.

(ii) Displacement alignment (lines 5–6)

This step is to align the translational displacement τ_1 and τ_2 between the rotation-normalized registered image

$f_\Theta(n_1, n_2)$ and the input image $g(n_1, n_2)$. The displacement parameters (τ_1, τ_2) can be obtained as the peak location of the POC function $\hat{r}^{M_1 M_2}_{f_\Theta g}(n_1, n_2)$. Then, we extend the size of the two images by τ_1 and τ_2 pixels for n_1 and n_2 directions, respectively, as shown in Fig. 7(c), in order to align the translational displacement between the two images. Thus, we have normalized versions of the registered image and the input image, which are denoted by $f'(n_1, n_2)$ and $g'(n_1, n_2)$.

(iii) Common region extraction (line 7)

Next step is to extract the overlapped region (intersection) of the two images $f'(n_1, n_2)$ and $g'(n_1, n_2)$. This process makes possible to improve the accuracy of fingerprint matching, since the non-overlapped areas of the two images become the uncorrelated noise components in the POC function. In order to detect the effective fingerprint areas for each image (the registered image $f'(n_1, n_2)$ or input image $g'(n_1, n_2)$), we examine the x-axis projection and the y-axis projection of pixel values. Only the common effective image areas, $f''(n_1, n_2)$ and $g''(n_1, n_2)$, of the two fingerprint images are extracted for the succeeding image matching step (Fig. 7(d)).

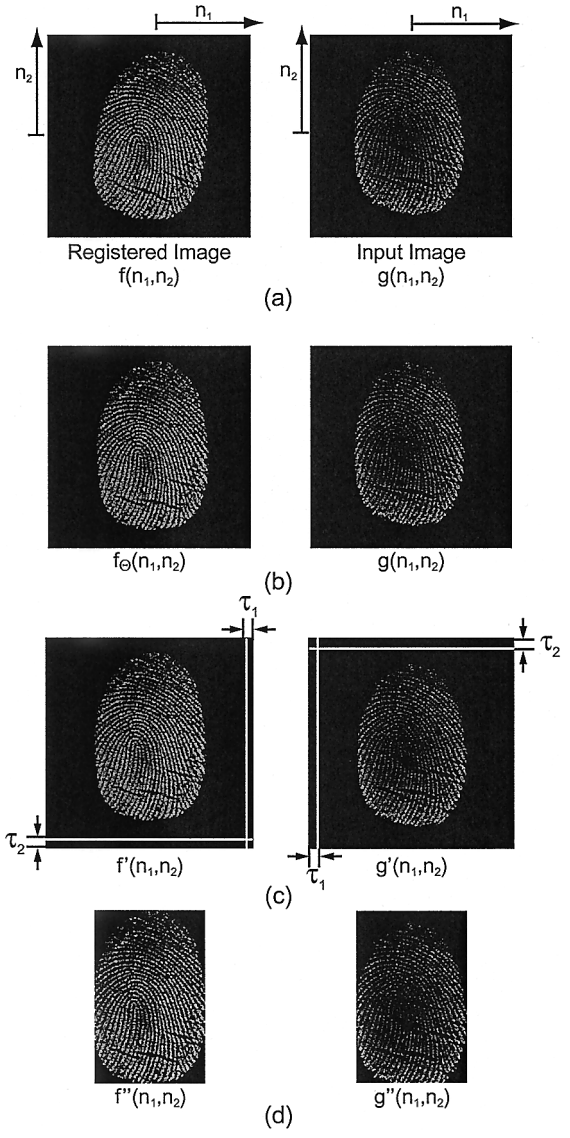

Fig. 7 Example of fingerprint matching using the proposed algorithm: (a) the registered fingerprint image $f(n_1, n_2)$ and the input fingerprint image $g(n_1, n_2)$, (b) rotation-normalized images $f_\Theta(n_1, n_2)$ and $g(n_1, n_2)$, (c) normalized images $f'(n_1, n_2)$ and $g'(n_1, n_2)$, and (d) common effective fingerprint regions $f''(n_1, n_2)$ and $g''(n_1, n_2)$.

(iv) Fingerprint matching (lines 8–10)

In this step, we first detect the inherent frequency band K_1 and K_2 from the 2D DFT of the registered fingerprint image $f''(n_1, n_2)$. Then, we calculate the band-limited POC function $\hat{r}^{K_1 K_2}_{f'' g''}(n_1, n_2)$ between the two images $f''(n_1, n_2)$ and $g''(n_1, n_2)$, and evaluate the matching score $S_P^{K_1 K_2}[f'', g'']$. As discussed earlier, the band-limited POC function gives multiple correlation peaks due to elastic fingerprint deformation. Thus, we need to introduce P-peak evaluation in computing the matching score $S_P^{K_1 K_2}[f'', g'']$. We use $P = 2$ in our experiments.

5. Experiments and Discussions

This section describes a set of experiments for evaluating fingerprint identification performance of the proposed algorithm.

In this experiment, we capture fingerprints using a fingerprint verification system (Yamatake Corporation, Prototype Version of "Friendtouch-Mini") shown in Fig. 8. This system [10] employs a pressure sensitive sensor, and can capture fingerprint images of 256×384 pixels. We expand the image size to 384×384 pixels for our matching algorithm.

We create a fingerprint database to compare identification performance between the proposed algorithm and the conventional algorithms. The subjects being tested are selected from 700 employees of a factory at Yamatake Corporation. From our experience, those who have difficult fingerprint is 3% of the total population. In order to compare the performance of the proposed algorithm and that of the conventional algorithms for difficult fingerprints, we select total of twelve subjects as follows: (i) eight of them are male and four are female, (ii) age range is from twenties to thirties,

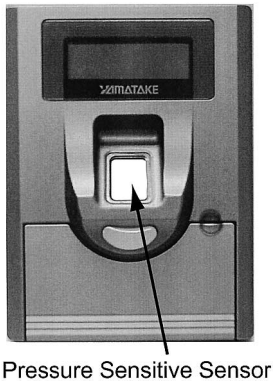

Fig. 8 Fingerprint verification system (developmental prototype version).

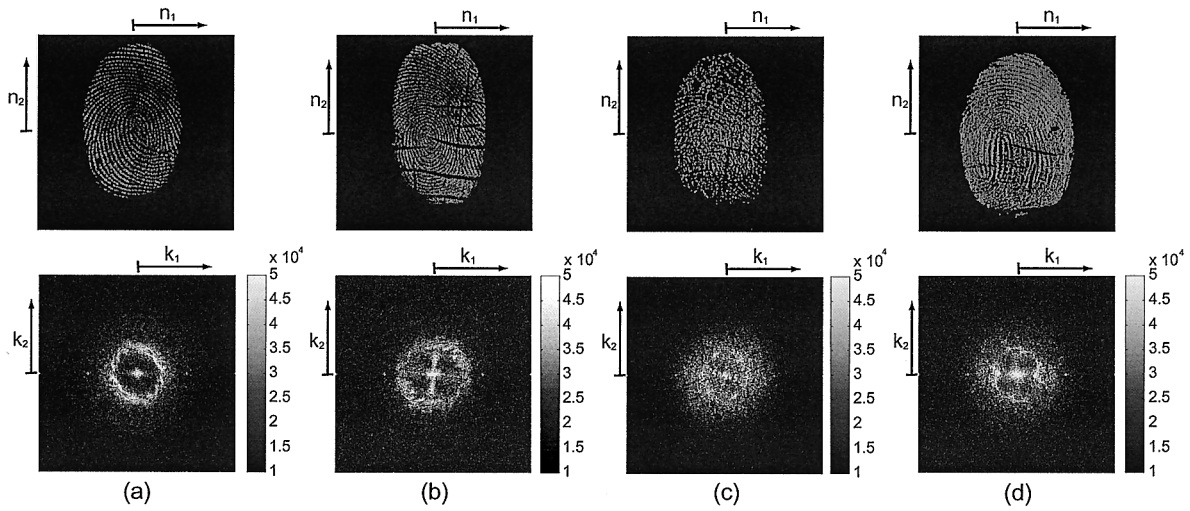

Fig. 9 Examples of fingerprint images in the database: (a) good quality fingerprint, (b) dry fingertip, (c) allergic skin disease and (d) rough fingertip.

(iii) seven of them have good quality fingerprints, three have dry fingertips, one has rough fingertip, and one has allergic skin disease. Thus, the test set considered here is specially designed to evaluate the performance of fingerprint matching algorithms under difficult condition.

Figure 9 shows some examples of fingerprint images in this database and the corresponding amplitude spectra. Figure 9(a) is a good-quality fingerprint, (b)–(d) are degraded fingerprints due to a dry fingertip, a rough fingertip and allergic skin disease. We can observe that the good quality fingerprint (Fig. 9(a)) has distinct minutiae points, while the degraded fingerprints (Figs. 9(b)–(d)) have some ambiguous minutiae points, which may cause serious miss-matching when using the minutiae-based matching algorithm. We expect that the proposed algorithm is more robust to such fingerprint degradation than the minutiae-based matching algorithm, since the POC-based matching employs global texture information rather than the small feature points. Also, the degraded fingerprints tend to contain random noise components in both high frequency domain and low frequency domain. Since the signal energy is significantly lower in high frequency domain, phase components are not reliable in high frequency domain. We can eliminate the effect of unreliable phase components in high frequency domain by using the band-limited POC function.

Registered fingers are right index fingers. The False Rejection Test (FRT) is to evaluate the False Rejection Rate (FRR) of fingerprint verification for every subject, where FRR is the probability that an authorized person is falsely rejected. For this purpose we capture 10 fingerprint images of the same right index finger for every subject, each of which is taken at different timing. These 10 fingerprint images must be passed by verification. The total number of fingerprint images used for FRT is 120 (12 subjects $\times$ 10 images).

On the other hand, the False Acceptance Test (FAT) is to evaluate the False Acceptance Rate (FAR) of fingerprint verification for every person, where FAR is the probability

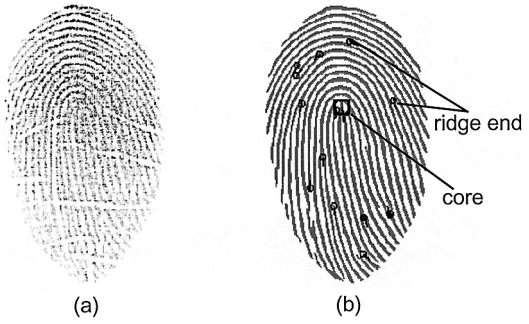

Fig. 10 Typical snapshots of the minutiae-based matching algorithm: (a) gray-scale normalization of a fingerprint image and (b) extraction of minutiae points (i.e., cores, deltas and ridge ends) after binarizing the fingerprint image.

that a non-authorized person is accepted as an authorized person. For every "genuine" target subject, we can consider 11 "impostors" in our experiment, and thus we capture 11 fingerprint images of right index fingers from the 11 impostor subjects. We also capture 12 fingerprint images of right middle fingers (different fingers) from all the subjects. For every genuine subject, these 23 fingerprint images must be rejected by verification. The total number of fingerprint images used for FAT is hence 276 (12 subjects $\times$ 23 images).

We compare three different matching algorithms: (A) the original POC-based algorithm without using band-limited POC function and common region extraction, (B) a typical minutiae-based algorithm (which is commercially available recently), and (C) the proposed algorithm. The minutiae-based matching algorithm used in this paper can be summarized as follows: (i) normalize the pixel value of the given fingerprint images to the range of [0,255] (Fig. 10(a)), (ii) extract the effective fingerprint region for the two images, (iii) enhance the fingerprint ridges, (iv) binarize the enhanced fingerprint images, (v) extract the three types of minutiae points, i.e., cores, deltas and ridge ends, from the

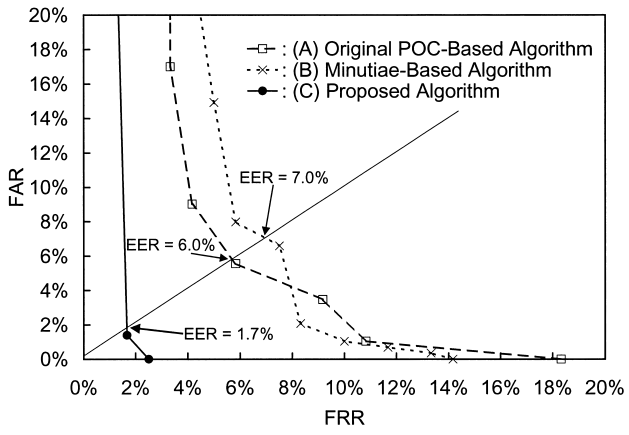

Fig. 11 ROC curve and EER.

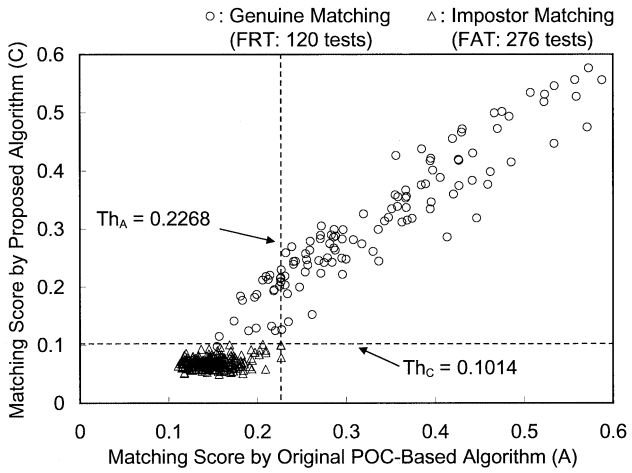

Fig. 12 Overall joint distribution of matching scores for the proposed matching algorithm and the original POC-based matching algorithm.

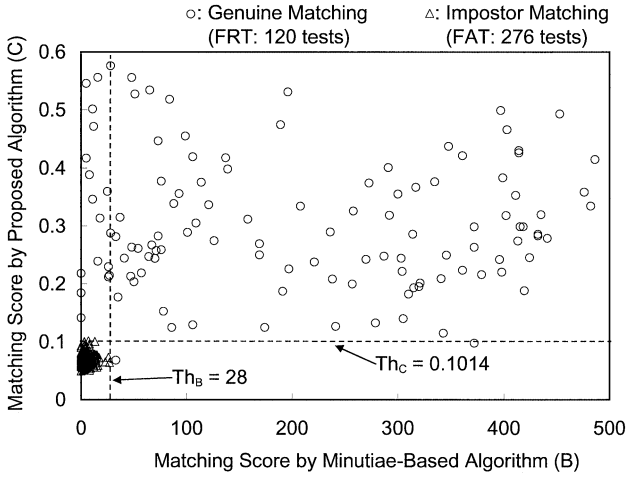

Fig. 13 Overall joint distribution of matching scores by the proposed algorithm and the minutiae-based matching algorithm.

binarized fingerprint images (Fig. 10(b)), and (vi) perform minutiae matching and evaluate the similarity between the two fingerprint images. The performance of the biometrics-based identification system is evaluated by the Receiver Operating Characteristic (ROC) curve, which illustrates the FAR against the FRR at different thresholds on the matching score. Figure 11 shows the ROC curve for the three algorithms (A)–(C). The proposed algorithm (C) exhibits significantly higher performance, since its ROC curve is located at lower FRR/FAR region than those of the original POC-based algorithm (A) and the minutiae-based algorithm (B). When FAR is zero, the FRR of the proposed algorithm is 2.5%, while the FRR of the original POC-based algorithm is 18.3% and that of the minutiae-based algorithm is 14.2%.

The Equal Error Rate (EER) provides a good indicator of system performance, which is defined as the error rate where the FAR and the FRR are equal. The EER of the proposed algorithm (C) is 1.7% while EER of the original POC-based algorithm (A) is 6.0% and that of minutiae-based algorithm (B) is 7.0%. As is observed in the above experiments, the proposed algorithm is particularly useful for verifying difficult fingerprint images.

Figures 12 and 13 shows actual joint distribution of matching scores for the three algorithms (A)–(C). Figure 12 compares the matching scores of the original POC-based algorithm (A) (horizontal axis) and those of the proposed algorithm (C) (vertical axis) for total 396 matching tests (120 FRTs plus 276 FATs). The vertical dashed line indicates the highest impostor's score of the original POC-based algorithm (A) and the horizontal dashed line indicates the highest impostor's score of the proposed algorithm (C). For these algorithms, we can observe clear correlation in their matching scores. In a practical fingerprint verification system, the highest impostor's score Th_A (or Th_C) is used as the threshold value of verification in order to guarantee the condition FAR = 0. Assuming this condition, we can observe that the original POC-based algorithm (A) accepts only 81.7% of genuine fingerprints and rejects the remaining 18.3%, while the proposed algorithm can accept 97.5% of genuine fingerprints and reject only 2.5% of them.

Similar comparison is performed between the typical minutiae-based algorithm (B) and the proposed algorithm (C) as shown in Fig. 13. In this case, no correlation is observed between the matching scores of the two algorithms, since these algorithms employ totally different matching criteria. When FAR = 0, the minutiae-based algorithm (B) accepts only 85.8% of genuine fingerprints and rejects the remaining 14.2%, while the proposed algorithm (C) achieves much higher acceptance rate 97.5%.

Figures 14, 15, 16 and 17 show the joint distribution of matching scores for two algorithms (B) and (C) depending on the quality of the registered fingerprints: *good quality* (seven images), *dry skin* (three images), *rough skin* (one image), and *allergic skin* (one image), respectively. Note that Fig. 13 combines these four figures (Figs. 14–17). When good-quality fingerprints are used as the registered fingerprints (Fig. 14), genuine matching always gives higher scores than impostor matching for both algorithms. When the degraded fingerprints are used as the registered fin-

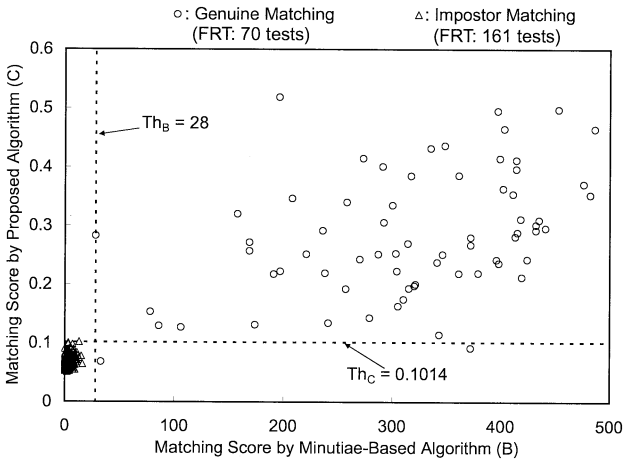

Fig. 14 Joint distribution of matching scores when *good-quality* fingerprints (seven images) are used as registered reference fingerprints.

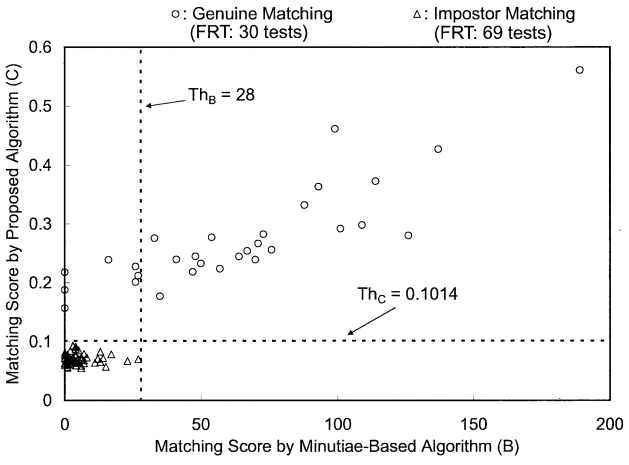

Fig. 15 Joint distribution of matching scores when *dry-skin* fingerprints (three images) are used as registered reference fingerprints.

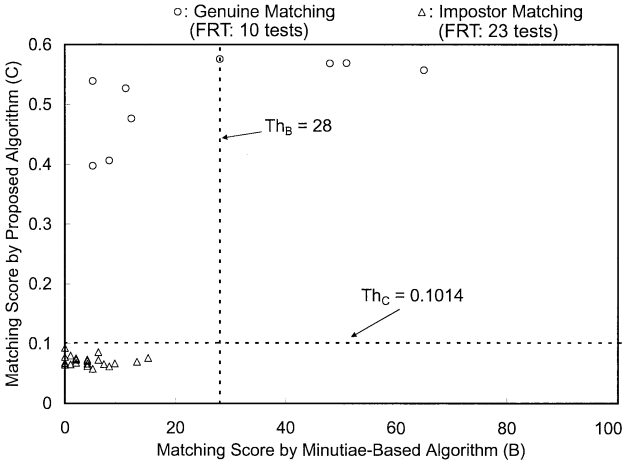

Fig. 16 Joint distribution of matching scores when a *rough-skin-condition* fingerprint (one image) is used as a registered reference fingerprint.

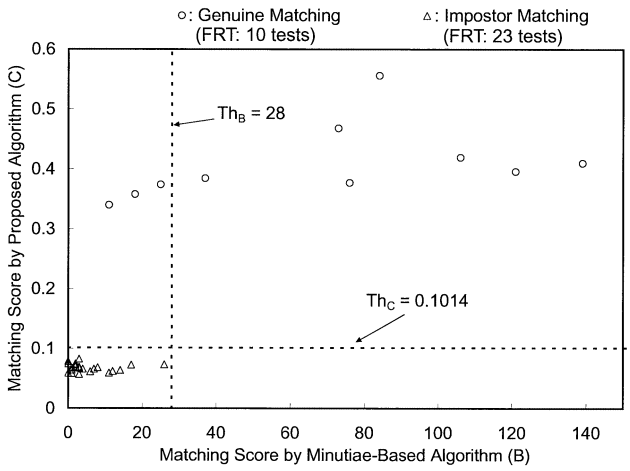

Fig. 17 Joint distribution of matching scores when an *allergic-skin* fingerprint (one image) is used as a registered reference fingerprint.

gerprints (Figs. 15–17), some genuine-matching scores are lower than impostor-matching scores for the minutiae-based matching algorithm (B). On the other hand, for the proposed algorithm (C), genuine matching always gives higher scores than imposter matching. This clearly demonstrates the excellent performance of the proposed algorithm for low quality fingerprint images.

6. Conclusion

This paper proposed an efficient fingerprint matching algorithm using the Phase-Only Correlation (POC) function. The proposed technique is particularly effective for verifying low-quality fingerprint images that could not be identified correctly by conventional techniques. It seems that the POC-based matching algorithm could be applied to other biometrics technologies, such as iris/retinal scanning, facial scanning and hand scanning.

References

[1] D. Maltoni, D. Maio, A.K. Jain, and S. Prabhakar, Handbook of Fingerprint Recognition, Springer, 2003.
[2] A.K. Jain, L. Hong, S. Pankanti, and R. Bolle, "An identity-authentification system using fingerprints," Proc. IEEE, vol.85, no.9, pp.1365–1388, Sept. 1997.
[3] D. Maio and D. Maltoni, "Direct gray-scale minutiae detection in fingerprints," IEEE Trans. Pattern Anal. Mach. Intell., vol.19, no.1, pp.27–40, Jan. 1997.
[4] C.D. Kuglin and D.C. Hines, "The phase correlation image alignment method," Proc. Int. Conf. on Cybernetics and Society, pp.163–165, 1975.
[5] H. Nakajima, K. Kobayashi, M. Kawamata, T. Aoki, and T. Higuchi, "Pattern collation apparatus based on spatial frequency characteristics (USP 5915034)," US Patent, May 1995.
[6] T. Aoki, T. Kenji, T. Higuchi, and K. Koji, "Phase-based image matching and its application to intelligent vision systems," Proc. Int. Symp. New Paradigm VLSI Computing, pp.95–100, Dec. 2002.
[7] Q. Chen, M. Defrise, and F. Deconinck, "Symmetric phase-only matched filtering of Fourier-Mellin transforms for image registration and recognition," IEEE Trans. Pattern Anal. Mach. Intell., vol.16, no.12, pp.1156–1168, Dec. 1994.

[8] T. Kenji, T. Aoki, Y. Sasaki, T. Higuchi, and K. Kobayashi, "High-accuracy subpixel image registration based on phase-only correlation," IEICE Trans. Fundamentals, vol.E86-A, no.8, pp.1925–1934, Aug. 2003.
[9] M.A. Muquit, T. Kenji, T. Aoki, and T. Higuchi, "High-accuracy passive 3D measurement using multi-camera system based on phase-only correlation," Proc. IEEE Int. Symp. Intelligent Signal Processing and Communication Systems, pp.91–95, Nov. 2002.
[10] http://www.aoki.ecei.tohoku.ac.jp/poc/

Koichi Ito received the B.E. degree in electronic engineering, and the M.S. degree in information sciences from Tohoku University, Sendai, Japan, in 2000 and 2002, respectively. He is currently working toward the Ph.D. degree. His research interest includes non-linear digital signal processing, computer graphics and biometric image processing. Mr. Ito received the Tohoku Section Presentation Award from Information Processing Society of Japan in 2000.

Hiroshi Nakajima received the B.E. degree in electronic engineering from Tohoku University, Sendai, Japan, in 1990. He is currently with Systems Development Department, Yamatake Corporation, Isehara, Japan. His research interest includes biometric image processing.

Koji Kobayashi received the B.E. and M.E. degrees in electronic engineering from Tohoku University, Sendai, Japan, in 1976, and 1978, respectively. He is currently a general manager of Vision Sensing Department, Yamatake Corporation, Isehara, Japan. His general interests includes real-time automation system architecture, network communication protocol LSI, biometric image processing, CMOS image sensor, and three-dimensional sensing.

Takafumi Aoki received the B.E., M.E., and D.E. degrees in electronic engineering from Tohoku University, Sendai, Japan, in 1988, 1990, and 1992, respectively. He is currently a Professor of the Graduate School of Information Sciences at Tohoku University. For 1997–1999, he also joined the PRESTO project, Japan Science and Technology Corporation (JST). His research interests include theoretical aspects of computation, VLSI computing structures for signal and image processing, multiple-valued logic, and biomolecular computing. Dr. Aoki received the Outstanding Paper Award at the 1990, 2000 and 2001 IEEE International Symposiums on Multiple-Valued Logic, the Outstanding Transactions Paper Award from the Institute of Electronics, Information and Communication Engineers (IEICE) of Japan in 1989 and 1997, the IEE Ambrose Fleming Premium Award in 1994, the IEICE Inose Award in 1997, the IEE Mountbatten Premium Award in 1999, and the Best Paper Award at the 1999 IEEE International Symposium on Intelligent Signal Processing and Communication Systems.

Tatsuo Higuchi received the B.E., M.E., and D.E. degrees in electronic engineering from Tohoku University, Sendai, Japan, in 1962, 1964, and 1969, respectively. He is currently a Professor at Tohoku Institute of Technology. From 1980 to 1993, he was a Professor in the Department of Electronic Engineering at Tohoku University. He was a Professor from 1994 to 2003, and was Dean from 1994 to 1998 in the Graduate School of Information Sciences at Tohoku University. His general research interests include the design of 1-D and multi-D digital filters, linear time-varying system theory, fractals and chaos in digital signal processing, VLSI computing structures for signal and image processing, multiple-valued ICs, multiwave opto-electronic ICs, and biomolecular computing. Dr. Higuchi received the Outstanding Paper Awards at the 1985, 1986, 1988, 1990, 2000 and 2001 IEEE International Symposiums on Multiple-Valued Logic, the Outstanding Transactions Paper Award from the Society of Instrument and Control Engineers (SICE) of Japan in 1984, the Technically Excellent Award from SICE in 1986, and the Outstanding Book Award from SICE in 1996, the Outstanding Transactions Paper Award from the Institute of Electronics, Information and Communication Engineers (IEICE) of Japan in 1990 and 1997, the Inose Award from IEICE in 1997, the Technically Excellent Award from the Robotics Society of Japan in 1990, the IEE Ambrose Fleming Premium Award in 1994, the Outstanding Book Award from the Japanese Society for Engineering Education in 1997, the Award for Persons of scientific and technological merits (Commendation by the minister of state for Science and Technology), the IEE Mountbatten Premium Award in 1999 and the Best Paper Award at the 1999 IEEE International Symposium on Intelligent Signal Processing and Communication Systems. He also received the IEEE Third Millennium Medal in 2000. He received the fellow grade from IEEE, IEICE, and SICE.